Triplet–Triplet Energy Transfer Controlled by the Donor–Acceptor Distance in Rigidly Held Palladium-Containing Cofacial Bisporphyrins

Sébastien Faure,[a, b] Christine Stern,[a] Enrique Espinosa,[a] Jasmin Douville,[b] Roger Guilard,*[a] and Pierre D. Harvey*[b]

Abstract: Eleven new complexes, including mono-, heterobi-, and homobimetallic cofacial bisporphyrins, (Pd)H$_2$DPS, (M)H$_2$DPX, (M)H$_2$DPB, (PdZn)DPS, (PdZn)DPX, (Pt)$_2$DPX, (M)$_2$DPB (M = Pd, Pt), and (Pt)P (DPS^{4-} = 4,6-bis[5-(2,8,13,17-tetraethyl-3,7,12,18-tetramethylporphyrinyl)]dibenzothiophene tetraanion, DPX^{4-} = 4,5-bis[5-(2,8,13,17-tetraethyl-3,7,12,18-tetramethylporphyrinyl)]-9,9-dimethyl-xanthene tetraanion, DPB^{4-} = 1,8-bis[5-(2,8,13,17-tetraethyl-3,7,12,18-tetramethylporphyrinyl)]biphenylene tetraanion, P^{2-} = 5-phenyl-2,8,13,17-tetraethyl-3,7,12,18-tetramethylporphyrin dianion) have been synthesized and characterized. The photophysical properties of the donor (M)P (M = Pd or Pt, P = porphyrin chromophore) and the acceptor (free base H$_2$P or (Zn)P)

depend on the C$_{meso}$–C$_{meso}$ distance and the presence of a heavy atom such as Pd^{II} or Pt^{II}. The data were compared with those for the known compounds (Pd)$_2$DPS, (Pd)$_2$DPX, H$_4$DPS, H$_4$DPX, H$_4$DPB, (Pd)P, (Zn)P, and H$_2$P. The rate constants for triplet–triplet energy transfer (k_{ET}) were measured for the heterobimetallic (PdZn) and monometallic [(M)H$_2$] derivatives (M = Pd, Pt). The fluorescence lifetimes ($\Delta \tau_F$) of the acceptors decrease as a result of the heavy-atom effect, and vary as follows: (Pd)H$_2$DPS ≪ (Pd)H$_2$DPX ∼ (Pd)H$_2$-DPB. The k_{ET} values calculated according to the equation $k_{ET} = (1/\tau_{emi} - 1/$

Keywords: donor–acceptor systems · energy transfer · palladium · photophysics · porphyrins

τ_{emi}^0), where τ_{emi}^0 is the emission lifetime of the homobimetallic bisporphyrins (no ET occurs), are equal to 0, 247 ± 57 and 133 ± 52 s^{-1} for DPS, DPX, and DPB, respectively, in the (Pd)H$_2$ series. These measurements allowed the range of distance over which the Dexter mechanism for T$_1$–T$_1$ energy transfer ceases to operate to be determined. This distance is somewhere between 4.3 and 6.3 Å, in agreement with our recent findings on singlet–singlet energy transfer. During the course of this study, the X-ray crystal structure for (Pd)H$_2$DPX was obtained; triclinic ($P\bar{1}$), $a = 11.1016(1)$, $b = 14.9868(2)$, $c = 20.6786(3)$ Å, $\alpha = 102.091(1)$, $\beta = 100.587(1)$, $\gamma = 101.817(1)°$, $V = 3199.19(7)$ Å^3, $Z = 2$.

[a] S. Faure, Dr. C. Stern, Dr. E. Espinosa, Prof. R. Guilard
LIMSAG UMR 5633, Université de Bourgogne
6 bd Gabriel, 21100 Dijon (France)
Fax: (+33) 380-396-117
E-mail: roger.guilard@u-bourgogne.fr

[b] S. Faure, J. Douville, Prof. P. D. Harvey
Département de Chimie de l'Université de Sherbrooke
Sherbrooke J1 K 2R1, Québec (Canada)
Fax: (+1) 81-9821-8017
E-mail: pierre.harvey@usherbrooke.ca

Supporting information for this article is available on the WWW under http://www.chemeurj.org/ or from the author. Comparison between Ct$_1$–Ct$_2$ and C$_{meso}$–C$_{meso}$ distances for several DPX systems. Comparison of the rate constants for triplet energy transfer for some porphyrin dimers.

Introduction

Knowledge of the photophysical properties of porphyrins and an understanding of the "communication" (such as energy transfer, electron transfer, and heavy-atom effect) between two porphyrin macrocycles are essential to explore the photosynthetic mechanism[1,2] and to elaborate advanced optoelectronic devices like optical gates, photoelectric cells, and sensors.[3–11] Numerous studies have focused on linear or planar molecular systems, but little work has been concerned with constrained systems in which a rigid spacer favors a cofacial geometry. An initial survey clearly showed that energy transfer (ET) increases as the distance between the donor and acceptor porphyrins decreases.[12] Energy-transfer mechanisms were analyzed by Dexter[13,14] and Förster[15] many years ago. Recently, our groups demonstrated that it is possible to determine the range of C$_{meso}$–C$_{meso}$ dis-

tance over which the Dexter and Förster mechanisms dominate in singlet–singlet energy transfer in cofacial donor–acceptor bisporphyrins. The cofacial bisporphyrin systems investigated included DPS, DPO (4,6-bis[5-(2,8,13,17-tetraethyl-3,7,12,18-tetramethylporphyrinyl)]dibenzofuran), DPA (1,8-bis[5-(2,8,13,17-tetraethyl-3,7,12,18-tetramethylporphyrinyl)]anthracene), DPX, and DPB for which the C_{meso}–C_{meso} distances have been determined by single-crystal X-ray diffraction data (Zn$_2$DPS: 6.33 Å,[16] H$_4$DPO: 5.53 Å,[17,18] H$_4$DPA: 4.94 Å,[19] H$_4$DPX: 4.32 Å,[17] and H$_4$DPB: 3.80 Å[18]). The rate constants for singlet–singlet energy transfer (k_{ET}) in these systems increase in the order DPS < DPO < DPA < DPX < DPB, which is consistent with the relative magnitudes of the C_{meso}–C_{meso} distances.
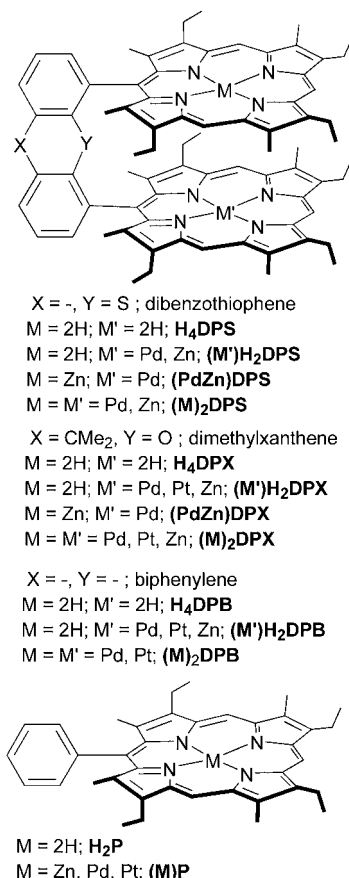
Contrary to singlet–singlet energy transfer, triplet–triplet energy transfer is characterized by the electronic exchange mechanism (Dexter) only.[20] This property allows luminescent devices controlled by interchromophore distances to be designed in which, at short C_{meso}–C_{meso} distances, energy transfer occurs with no or low luminescence observed from the donor, and at long C_{meso}–C_{meso} separations, efficient energy transfer cannot be accurately detected as one reaches the limit of accuracy of the lifetime or intensity change measurements and a maximum luminescence intensity is detected from the donor. Only a few porphyrin dimers have been investigated,[6,21–25] none of which contained a cofacial geometry. In such cases, direct π–π orbital overlapping is necessary.[5,26] For β-substituted porphyrins (such as those investigated in this work), the electron density located at the *meso*-carbon atoms on the frontier MOs is very small.[27–30] As a consequence, energy transfer cannot operate efficiently through the chemical bonds. Consequently, through-space processes are anticipated. It is well known that the DPB bisporphyrin systems exhibit the shortest cofacial separation and hence should promote more efficient through-space triplet–triplet energy transfer. This "on–off" situation for energy transfer, which is controlled by a change in cofacial interchromophore distance, is unprecedented.

We now report the synthesis and characterization of three triplet–triplet donor–acceptor cofacial bisporphyrin systems in which DPS, DPX, and DPB are used as spacers. The choice of these systems is based on our previous findings for singlet–singlet energy transfer: the Förster mechanism dominates in the DPS system, while for DPB, the Dexter mechanism is more important. Finally, the DPX spacer has an intermediate C_{meso}–C_{meso} distance and rate constant for energy transfer. We have elected to investigate the highly phosphorescent (Pd)*P* and (Pt)*P* chromophores,[6,31] which means that the ππ* triplet state is well populated. Also, these chromophores have numerous applications in the sensorization of O$_2$.[32–34] The fluorescence data are complicated because of the heavy-atom effect,[20,35] but this perturbation as well as the rate constant for triplet–triplet energy transfer are dependent on the C_{meso}–C_{meso} distance. The approximate distance at which T$_1$–T$_1$ energy transfer (Dexter mechanism) in cofacial bisporphyrins becomes negligible (too small to be detected) is determined to be between 4.3 and 6.2 Å which

is in good agreement with previous findings on S$_1$–S$_1$ energy transfer.

Results

Synthesis: The compounds investigated in this work are shown in Scheme 1. Homobimetallic bisporphyrins (Pd)$_2$DPB, (Pt)$_2$DPB, and (Pt)$_2$DPX were obtained in good

X = - , Y = S ; dibenzothiophene
M = 2H; M' = 2H; **H$_4$DPS**
M = 2H; M' = Pd, Zn; **(M')H$_2$DPS**
M = Zn; M' = Pd; **(PdZn)DPS**
M = M' = Pd, Zn; **(M)$_2$DPS**

X = CMe$_2$, Y = O ; dimethylxanthene
M = 2H; M' = 2H; **H$_4$DPX**
M = 2H; M' = Pd, Pt, Zn; **(M')H$_2$DPX**
M = Zn; M' = Pd; **(PdZn)DPX**
M = M' = Pd, Pt, Zn; **(M)$_2$DPX**

X = - , Y = - ; biphenylene
M = 2H; M' = 2H; **H$_4$DPB**
M = 2H; M' = Pd, Pt, Zn; **(M')H$_2$DPB**
M = M' = Pd, Pt; **(M)$_2$DPB**

M = 2H; **H$_2$P**
M = Zn, Pd, Pt; **(M)P**

Scheme 1. Mono- and bisporphyrins investigated in this work.

yields by the reaction of the corresponding non-metalated bisporphyrins with an excess of PdCl$_2$ or PtCl$_2$. However, this methodology cannot be applied to the synthesis of (Pd)H$_2$DPB, (Pd)H$_2$DPS, (Pd)H$_2$DPX, (Pt)H$_2$DPB, and (Pt)H$_2$DPX. In these cases, stoichiometric reactions led to a mixture of mono- and dimetalated products, along with the starting material, with the desired monopalladium(ii) (or monoplatinum(ii)) bisporphyrins being produced in only very small quantities. The use of monozinc(ii) bisporphyrins[36] as starting materials in the presence of >1 equiv of PdCl$_2$ (or PtCl$_2$) gave better results ((PdZn) derivatives: yield 37–53%; Scheme 2). Zinc is used as a protecting group for one of the two macrocycles and is removed by the H$^+$ ions generated during the reaction.[37] Small quantities of di-
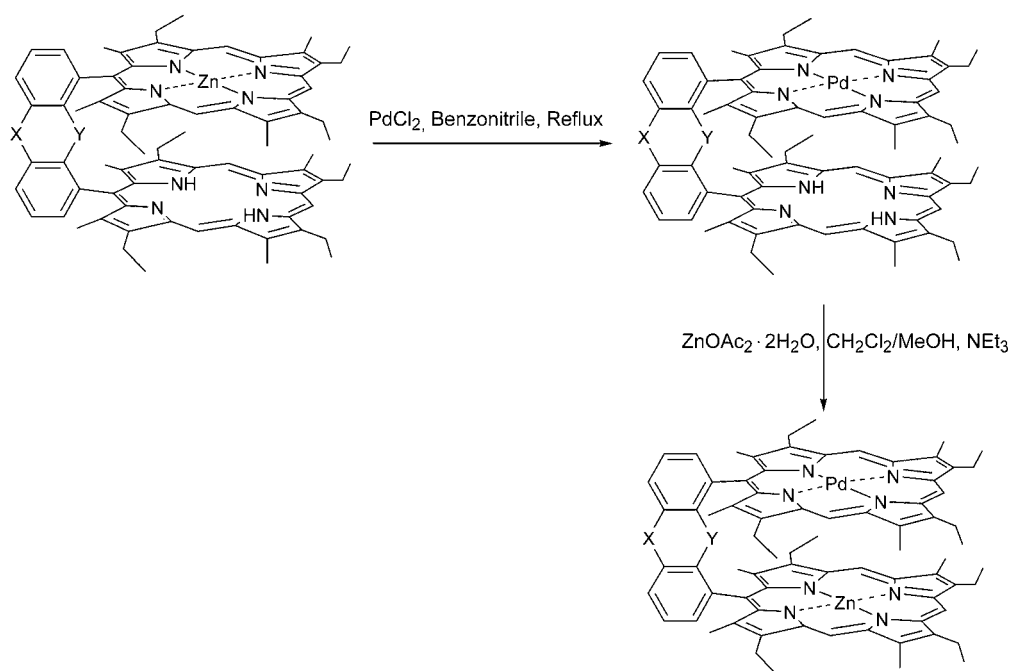
Scheme 2. Synthesis of (Pd)H$_2$ and (PdZn) bisporphyrins.

palladium(II) (or diplatinum(II)) bisporphyrins were also observed. For the palladium derivatives, in the presence of a base used to neutralize the excess H$^+$ ions, the reactions led to a mixture that contained both bis(palladium) and mixed-metal palladium(II)–zinc(II) bisporphyrins. This methodology was not further investigated. Instead, the mixed-metal species were prepared from the metalation of the mono-palladium(II) bisporphyrins by using zinc acetate. All compounds were characterized by ^{1}H NMR spectroscopy, elemental analysis, and MALDI-TOF mass spectrometry.

Crystallographic data: The crystallographic data for (Pd)H$_2$DPX are summarized in Table 1 and the molecular structure is shown in Figure 1. The parameters describing its molecular geometry (Figure 2) are given in Table 2. (Pd)H$_2$DPX exhibits the expected cofacial structure. The palladium atom is found to be disordered with an occupancy of 0.5 per macrocycle. For the sake of discussion, it is arbitrarily assigned to only one macrocycle (macrocycle 1). The peripheral ethyl groups located away from the spacer are also disordered in one macrocycle. With an occupancy close to 0.5, these groups either face outward or inward with respect to the geometry of the cofacial bismacrocycle. In addition, the corresponding pyrrole rings are also disordered; the averaged pyrrole plane deviates by about 2° irrespective of whether the ethyl groups are oriented outward or inward.

The palladium atom is placed at the center of the porphyrin ring, and the distance between the calculated center of the four nitrogen atoms (the centroid position, Ct) and the palladium atom is less than 0.03 Å. The porphyrin macrocycle is relatively planar as the maximum deviation between any atom and the averaged carbon plane is 0.17 Å;

Table 1. Crystal data and structure refinement for (Pd)H$_2$DPX.

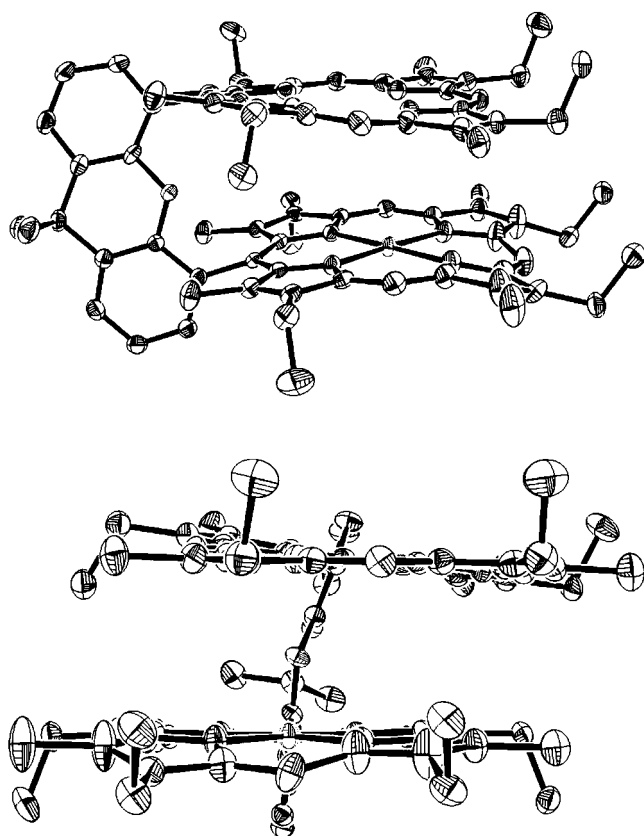|	(Pd)H$_2$DPX
formula	C$_{79}$H$_{84}$N$_8$OPd
formula weight	1267.94
temperature [K]	110(2)
wavelength [Å]	0.71069
crystal system	triclinic
space group	P$\bar{1}$
unit cell dimensions	
a [Å]	11.1016(1)
b [Å]	14.9868(2)
c [Å]	20.6786(3)
α [°]	102.091(1)
β [°]	100.587(1)
γ [°]	101.817(1)
volume [Å^3]	3199.19(7)
Z	2
ρ_{calcd} [Mg m^{-3}]	1.316
μ [mm^{-1}]	0.344
$F(000)$	1336
crystal size [mm^3]	0.50 × 0.37 × 0.10
θ range for data collection [°]	1.96–27.36
index ranges	$-14 \leq h \leq 13$, $-19 \leq k \leq 19$, $-25 \leq l \leq 26$
reflections collected	25 195
independent reflections	14 360 [R(int) = 0.0578]
completeness to θ_{max} [°]	98.9 % [$\theta = 27.36$]
absorption correction	none
refinement method	full-matrix least-squares on F^2
data/restraints/parameters	14 360/18/899
goodness-of-fit on F^2	1.132
final R indices [$I > 2\sigma(I)$]	$R_1 = 0.0693$, $wR_2 = 0.1352$
R indices (all data)	$R_1 = 0.1173$, $wR_2 = 0.1474$
extinction coefficient	0.0065(4)
largest diff. peak and hole [eÅ^{-3}]	0.560 and -1.034

Figure 1. Crystal structure of (Pd)H$_2$DPX. Hydrogen atoms are omitted for clarity. Thermal ellipsoids are drawn at the 50% probability level.
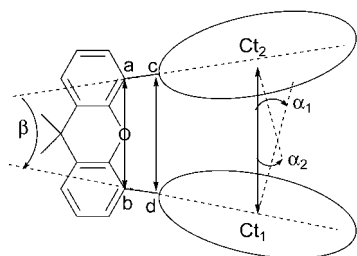

Figure 2. Illustration of the crystallographically derived geometrical features.

for palladium, this deviation is only 0.09 Å. The angle formed by the two averaged porphyrin planes (β) is only 5.4°, which indicates that the rings are fairly parallel. The values of the lateral shift ($S_p = 1.71$ Å) and slip angle ($\alpha = (\alpha_1 + \alpha_2)/2 = 25.3°$) further indicate the potential displacement between both rings. The large slip angle is due, in part, to the large angle formed between the two benzene rings ($\gamma = 15°$). Nocera and co-workers have also reported a large deviation for this spacer.[17] For the DPX systems, this angle is 36° for the free base, and 6–15° for the dimetalated bisporphyrins. Such large deviations have not been reported for other spacers such as anthracenyl, biphenylenyl, and dibenzofuran.[17,38] The C$_{meso}$–C$_{meso}$ (4.32 Å) and Ct$_1$–Ct$_2$

Table 2. Crystallographically derived geometrical features of (Pd)H$_2$DPX.

Parameters	Value
α_1 [°]	24.6
α_2 [°]	25.9
α(slip angle $= (\alpha_1 + \alpha_2)/2$) [°]	25.3
β(interplanar angle) [°]	5.4
γ(spacer angle) [°]	14.8
d_{a-b} [Å]	4.61
d_{c-d} [Å]	4.32
$d_{Ct1-Ct2}$ [Å]	4.01
$d_{Ct1-Pd1}$[a] [Å]	0.03
$d_{Ct2-Pd1}$[b] [Å]	3.98
S_p (lateral shift $= d_{Ct1-Ct2}\sin\alpha$) [Å]	1.71
S_r (intermacrocycle separation $= d_{Ct1-Ct2}\cos\alpha$) [Å]	3.63

[a] Distance between the centroid (Ct) and palladium atom in the same macrocycle. [b] Distance between the first macrocycle centroid (Ct) and the palladium atom in the other macrocycle.

(4.01 Å) distances determined in this work compare favorably with those of other DPX systems (4.27 Å $<$ C$_{meso}$–C$_{meso}$ $<$ 4.47 Å; 3.87 Å $<$ Ct$_1$–Ct$_2$ $<$ 4.70 Å; see the Supporting Information).[17,39,40]

Absorption spectra: The UV/Vis absorption data are reported in Table 3 and the spectra for (Pd)H$_2$DPS, (Pd)H$_2$DPX, (Pd)H$_2$DPB, (PdZn)DPS, (PdZn)DPX, (Pt)H$_2$DPX, and (Pt)H$_2$DPB are shown in Figure 3. For the palladium derivatives, the Soret band λ_{max} (S$_0$–S$_2$ transition) varies as a function of the spacer in the order DPS $>$ DPX $>$ DPB. A decrease in the absorptivity of the Soret band was also observed. Both the shift and the intensity decrease as the C$_{meso}$–C$_{meso}$ distance decreases. The Q bands (S$_0$–S$_1$ transition) also exhibit a slight shift to the red in the same order.[41] For (Pt)H$_2$DPX and (Pt)H$_2$DPB, the absorption spectra are nearly the same.

Luminescence: The photophysical data for all the compounds studied are summarized in Table 4 and Table 5 and the emission spectra are shown in Figures 4, 6, and 7. Four chromophores were investigated, H$_2$P and (Zn)P, known to be strongly fluorescent,[27,42] and (Pd)P and (Pt)P, which are strongly phosphorescent.[27,43] For mixed chromophore systems, both types of emission were observed. At 298 K, (Pd)P showed no detectable luminescence, which contrasts with other palladium(II) porphyrin systems.[34,43]

The 298 K emission spectra of (Pd)H$_2$DPS and (Pd)H$_2$DPX (Figure 4a) exhibit the same spectral signature as that of H$_2$P fluorescence. The luminescence of the (Pd)P chromophore can be easily distinguished from the H$_2$P fluorescence by time-resolved spectroscopy by taking advantage of the very different emission lifetimes (for (Pd)P $\tau_{em} \sim 100$–550 μs). The emission spectrum of (Pd)H$_2$DPB exhibits two luminescence bands as well (Figure 4a) due to the fluorescence of the H$_2$P chromophore ($\lambda_{0,0} \approx 640$ nm) and the phosphorescence of the (Pd)P chromophore ($\lambda_{0,0} = 663$ nm). The $\lambda_{0,0}$ of the H$_2$P fluorescence follows the same trend as that of the absorption: $\lambda_{0,0}$(DPS) $= 628$ nm $< \lambda_{0,0}$(DPX) $=$

Table 3. UV/Vis absorption data in CH_2Cl_2 at 298 K.

Compound	Soret region		λ_{max} [nm] ($\varepsilon \times 10^{-3}$ M^{-1} cm^{-1}) Q bands		
H_2P	402 (154)	502 (15)	532 (8)	578 (6)	626 (4)
$(Zn)P$	410 (270)	540 (18)		576 (11)	
$(Pd)P$	398 (180)	504 (16)		538 (43.2)	
$(Pt)P$	394 (209)	502 (10.2)		537 (30.9)	
H_4DPS	398 (309.9)	502 (29.6)	536 (15.0)	570 (14.2)	622 (6.8)
$(Zn)H_2DPS$	402 (340.6)	502 (15.6)	534 (21.7)	570 (20.9)	624 (3.1)
$(Pd)H_2DPS$	394 (402.8)	509 (29.5)	571 (12.8)	549 (40.7)	624 (4.9)
$(Zn)_2DPS$	402 (473.6)	536 (32)		572 (29)	
$(Pd)_2DPS$[41]	394 (256.9)	516 (23.5)	548 (44.7)	610 (0.29)	
$(PdZn)DPS$	395 (304.7)	515 (20.2)	549 (39.9)	573 (9.2)	
H_4DPX	380 (200)	508 (12.0)	543 (5.4)	578 (6.0)	628 (3.3)
$(Zn)H_2DPX$	386 (268)	512 (9.5)	542 (11.7)	576 (12.0)	628 (2.0)
$(Pd)H_2DPX$	383 (298.5)	515 (16.4)	554 (19.3)	579 (9.8)	628 (1.9)
$(Pt)H_2DPX$	377 (157.9)	507 (4)	540 (9.5)	574 (4.3)	627 (1)
$(Zn)_2DPX$[17]	389 (290)	541 (14.3)		576 (13.2)	
$(Pd)_2DPX$[41]	386 (265.2)	520 (16.7)	552 (31.3)	614 (0.17)	
$(Pt)_2DPX$	374 (170.3)	509 (8.4)		541 (21.5)	
$(PdZn)DPX$	387 (266.6)	526 (9.9)	556 (11.1)	579 (4.7)	
H_4DPB	379 (173.9)	511 (6.3)	540 (2.0)	580 (3.4)	632 (1.8)
$(Zn)H_2DPB$[36]	388 (200.0)	518 (4.1)	542 (5.2)	581 (6.8)	633 (0.8)
$(Pd)H_2DPB$	382 (217.5)	516 (9.9)	556 (11.1)	579 (4.7)	
$(Pt)H_2DPB$	376 (173.2)	508 (9.5)	544 (12.5)	578 (3)	632 (1.7)
$(Pd)_2DPB$	383 (270.5)	521 (19.0)		553 (35.8)	
$(Pt)_2DPB$	373 (63)	511 (3.3)		542 (8.3)	

636 nm $< \lambda_{0,0}$(DPB) ≈ 640 nm. At 77 K (Figure 4b), $(Pd)P$ is phosphorescent ($\lambda_{0,0} = 659$ nm). For the three mixed-metal compounds, both fluorescence of the H_2P chromophore and phosphorescence of the $(Pd)P$ moiety were observed. However, the relative intensities vary significantly depending on the spacer. For instance, H_2P fluorescence is more important in $(Pd)H_2DPS$, while $(Pd)H_2DPB$ exhibits a strong $(Pd)P$ phosphorescence. A qualitative energy diagram for the mono-palladium bisporphyrins has been established by using the positions of the 0–0 peaks in the absorption and fluorescence spectra, the maxima of the $(Pd)P$ phosphorescence spectra, and the energy of the H_2P triplet state (Figure 5).[44] From this, one finds that the energies decrease in the order $^1(Pd)P > {}^1H_2P > {}^3(Pd)P > {}^3H_2P$. Similarly, by using the 0–0 absorption and fluorescence data and the maxima of the phosphorescence bands of the $(Pd)P$ and $(Zn)P$ chromophores in the palladium-zinc bisporphyrins (Figure 6), a qualitative energy diagram can be derived: $^1(Pd)P > {}^1(Zn)P > {}^3(Pd)P > {}^3(Zn)P$ (Figure 5). Similarly, one also finds for the platinum systems that $^1(Pt)P > {}^1H_2P > {}^3(Pt)P > {}^3H_2P$. The relative $(Pd)P$ phosphorescence intensity of $(PdZn)DPS$ is large compared with that of the fluorescence and phosphorescence of $(Zn)P$ (Figure 6a).[27,28] On the other hand, the intensity of the $(Pd)P$ phosphorescence is of the same order of magnitude as the $(Zn)P$ fluorescence and phosphorescence of the DPX system.

The emission spectra of $(Pt)H_2DPX$ and $(Pt)H_2DPB$ are compared with that of $(Pt)P$ in Figure 7. The H_2P fluorescence is entirely blurred by the $(Pt)P$ phosphorescence at both 298 and 77 K. Interestingly, the H_2P phosphorescence, an emission rarely reported in the literature,[44] becomes visi-

ble in the region of 750–850 nm, with maxima at 794 and 824 nm.

Overall, these data are indicative of triplet–triplet energy transfer between $^3(Pd)P^*$ and $^3H_2P^*$, $^3(Pt)P^*$ and $^3H_2P^*$, and $^3(Pd)P^*$ and $^3(Zn)P^*$, but the nature of the spacer plays a crucial role. For accuracy, the rate constants for triplet–triplet energy transfer were measured by using the phosphorescence lifetimes (Table 5).[24,45–47] The fluorescence lifetimes of the H_2P and $(Zn)P$ chromophores are in the expected ns range (1–24 ns for the H_2P chromophore and 1–2 ns for the $(Zn)P$ chromophore).[6] Similarly, the phosphorescence lifetimes (τ_P) of the $(Pd)P$ chromophore in the porphyrin systems are predictably in the μs range but vary greatly with the temperature and the nature of the spacer. Further evidence for triplet–triplet energy transfer comes from a comparison of the phosphorescence quantum yields (Φ_P; Table 4).

Discussion

Singlet excited states and fluorescence: The relative order of the singlet-state energies established from the 0–0 peaks observed in the absorption and fluorescence spectra, $^1(Pd)P$ and $^1(Pt)P > {}^1(Zn)P \gg {}^1H_2P$, indicates that the $^1(Pd)P$ and $^1(Pt)P$ $\pi\pi^*$ states are the most energetic. These chromophores can act as donors for singlet–singlet energy transfer, $^1(Pd)P^* \rightarrow {}^1(Zn)P^*$, $^1(Pd)P^* \rightarrow {}^1H_2P^*$, and $(Pt)P^* \rightarrow {}^1H_2P^*$, but such a process if present, cannot be investigated in this work since the fluorescence of $(Pd)P$ and $(Pt)P$ chromophores are totally blurred by the much stronger fluorescence of the H_2P or $(Zn)P$ chromophore (Figures 4, 6, and 7).[48]

The values of τ_F (298 K) for the H_2P chromophore in H_2P, H_4DPS, H_4DPX, and H_4DPB decrease in the following order: $H_2P \sim H_4DPS > H_4DPX > H_4DPB$. In our previous paper, such a sequence for a series of five spacers (H_4DPS, H_4DPO, H_4DPA, H_4DPX, and H_4DPB) was interpreted as follows.[12] The shorter lifetimes are a consequence of intramolecular macrocycle–macrocycle interactions or collisions that promote nonradiative deactivation. This phenomena is also exhibited by the mono-palladium series $(Pd)H_2DPS$, $(Pd)H_2DPX$, and $(Pd)H_2DPB$ as illustrated in Figure 8. Comparison of this monopalladium series with the non-metalated one (Figure 8) indicates that the τ_F values for the fluorescence of the H_2P chromophore are always smaller for
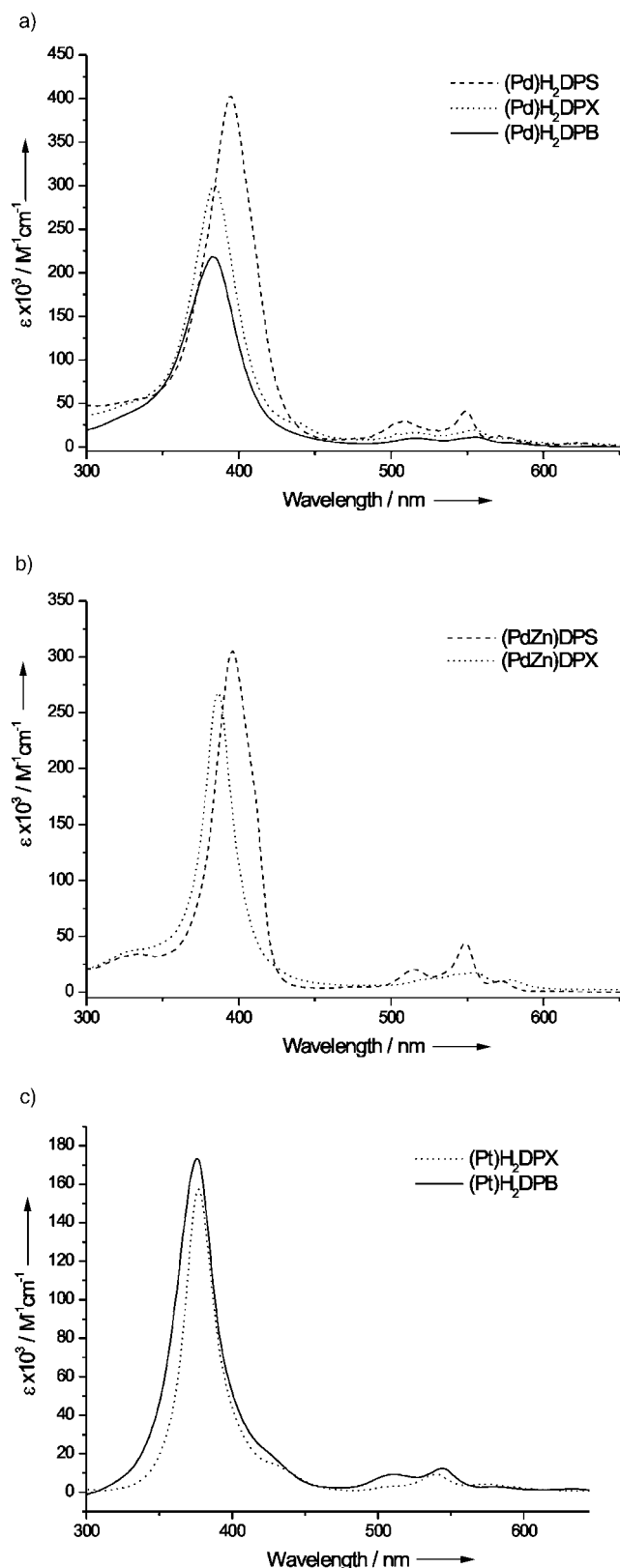
a)

b)

c)

Figure 3. UV/Vis spectra of a) (Pd)H$_2$-, b) (PdZn)-, and c) (Pt)H$_2$-bisporphyrins (298 K, CH$_2$Cl$_2$).

the monopalladium series. This behavior can be explained by the intermolecular "heavy-atom effect" due to the palla-

dium atom.[20,35] The most important feature is that the difference between τ_F for the non-metalated and monopalladium members of the series (H$_2$P, $\Delta\tau_F$) is more significant for (Pd)H$_2$DPB than for (Pd)H$_2$DPS (i.e. $\Delta\tau_F$ increases in the order DPS < DPX < DPB). This result is consistent with the change in interchromophoric separation between the H$_2$P lumophore and the (Pd)P macrocycle.[49] This interpretation contrasts with the results obtained for (PdZn)DPS (τ_F[(Zn)P] = 2.0 (298 K) and 1.8 ns (77 K)) and (PdZn)DPX (τ_F[(Zn)P] = 1.9 (298 K) and 2.1 ns (77 K)), which appear to be insensitive to the presence of palladium compared with the corresponding bis-zinc bisporphyrins (Zn)$_2$DPS (τ_F[(Zn)P] = 1.95 (298 K) and 1.85 ns (77 K)) and (Zn)$_2$DPX (τ_F[(Zn)P] = 1.7 (298 K) and 1.9 ns (77 K)).[12] This apparent nonsensitivity may be due to the fact that zinc exhibits a small spin–orbit coupling constant which induces some intramolecular "heavy-atom effect". Consequently the rate of intersystem-crossing in the (Zn)P intrachromophore may be important enough to render the interchromophore ((Zn)P versus (Pd)P) "heavy-atom effect" negligible.

Triplet-excited states and energy transfer: As already stated, the phosphorescence arising from the (Pd)P chromophore is readily detected in all cases. Comparison of the τ_P data at 298 K for (Pd)P, (Pd)$_2$DPS, (Pd)$_2$DPX, and (Pd)$_2$DPB (Table 5 and Figure 9) shows that values of τ_P increase from (Pd)P to (Pd)$_2$DPS and to (Pd)$_2$DPX, and then decrease for (Pd)$_2$DPB. This variation in data can be attributed to the efficient nonradiative deactivation of the ^{3}(Pd)P state.[50] Nocera and co-workers[34] recently noticed a similar dependence of the photophysical properties of (Pd)P(BrPhEtio), (Pd)$_2$DPO, and (Pd)$_2$DPX. Their interpretation of the data based on DFT computations indicated that a torsional distortion along the C$_{meso}$–C$_{aryl}$ bond, accompanied by a nonplanar distortion of the macrocyclic framework, induces an significant decrease in the T$_1$–S$_0$ energy gap. As the macrocycle is less constrained, the porphyrin rings have greater scope for framework distortion. Consequently, the greater the molecular distortion in the triplet state, the lower the energy of the triplet state. This allows a more efficient nonradiative deactivation of the T$_1$ state. Similarly, Albinsson and co-workers performed other DFT calculations on zinc and free-base bis(5,15-diaryloctaalkylporphyrin) for which unusual triplet-state dynamics were observed.[51] They concluded that distortions along the C$_{meso}$–C$_{aryl}$ bond and of the macrocycle plane (saddle-shaped conformation) have induced a change in conformation of the T$_1$ state. With regards to the present study, the observed increase in τ_P on going from (Pd)P to (Pd)$_2$DPS to (Pd)$_2$DPX parallels the increase in τ_P observed for (Pd)(BrPhEtio)P to (Pd)$_2$DPO to (Pd)$_2$DPX by Nocera and co-workers. However, (Pd)$_2$DPB behaves differently as τ_P decreases. In this case, the shorter C$_{meso}$–C$_{meso}$ distance indicates stronger intermacrocycle interactions and greater π–π contacts, which promote more efficient nonradiative T$_1$ deactivation. Our groups recently observed this phenomena in the fluorescence spectra at 298 and 77 K for the free-base series H$_2$DPS, H$_2$DPO, H$_2$DPA,

Table 4. Luminescence data.[a]

Compound macrocycle	metal or H	λ_{max} [nm][b] 298 K	77 K	Quantum yields[c] 298 K	77 K
P	2H[d]	629, 696	623, 690	0.0892	0.0862
	Zn	580, 635	581, 639, 721	0.0214	0.0266
	Pd	–	659, 691, 712, 731	–	0.5576
	Pt	649	640	0.0049	0.8364
DPS	4H[d]	629, 697	623, 689	0.0887	0.0838
	Pd, 2H[e]	628, 696	621, 661, 689	0.0809	0.1370
	2Pd	669	660, 694, 713, 735	0.0018	0.1052
	Zn, Pd[e]	580, 634, 668	582, 660, 694, 714, 735	0.0681	0.2736
DPX	4H[d]	635, 701	637, 702	0.0361	0.0643
	Pd, 2H[e]	636, 703	632, 665, 700	0.0035	0.0101
	Pt, 2H[e]	645, 703	645, 701, 794, 824	0.0014	0.0030
	2Pd	674	668, 745	0.0623	0.3811
	2Pt	652	648	0.0744	0.1470
	Zn, Pd[e]	591, 643, 670	566, 595, 643, 658, 683, 742, 820	0.0691	0.0182
DPB	4H[d]	641[18]	636[18]	0.0040[18]	0.012[18]
	Pd, 2H[e]	663, 708	633, 658	0.0140	0.0346
	Pt, 2H[e]	647	648, 794, 824	0.0233	0.0075
	2Pd	665	667	<0.001	0.1936
	2Pt	652	648	0.0168	0.0910

[a] In 2-MeTHF, $\lambda_{excitation} = 510$ nm; the quantum yield was evaluated by reference to H_2TPP $(0.11)^{[27,42,63]}$ and the quantum yield for H_2TPP (0.11) at 77 K was verified by reference to (Pd)TPP (0.17; 77 K; MCH).[43,64] [b] The uncertainties in the values of λ_{max} are ±1 nm. [c] The uncertainties in the values of the quantum yields are ±10%. [e] The total quantum yield and porphyrin's absorbances arise from the two chromophoric species. [d] $\lambda_{excitation} = 500$ nm.

Table 5. Fluorescence lifetimes and rate constants for triplet–triplet energy transfer.[a]

Compound macrocycle	metal or H	chromophore	Lifetime (298 K)[b] τ_F [ns]	τ_P [μs]	Lifetime (77 K)[b] τ_F [ns]	τ_P [μs]	k_{ET} (77 K) [s^{-1}]
P	2H	free base	17.3	–	23.3	–	–
	Zn	(Zn)P	1.7	[c]	1.94	[c]	–
	Pd	(Pd)P	[c]	25	[c]	1870	–
	Pt	(Pt)P	–	18	–	128	–
DPS	4H	free base	18.0	–	23.6[18]	–	–
	Pd, 2H	free base	17.6	–	23.6	–	
		(Pd)P	[c]	98	[c]	1920	0
	2Pd	(Pd)P	[c]	210	[c]	1920	–
	Zn, Pd	(Zn)P	2.0	[c]	1.75	[c]	
		(Pd)P	[c]	98	[c]	1920	0
DPX	4H	free base	14.1	–	17.0[18]	–	–
	Pd, 2H	free base	12.0	–	15.2	–	
		(Pd)P	[c]	568	[c]	1440	247
	Pt, 2H	free base	12	–	–	559	
		(Pt)P	–	40.6	–	126	2220
	2Pd	(Pd)P	[c]	440	[c]	2240	–
	2Pt	(Pt)P	–	46	–	175	
	Zn, Pd	(Zn)P	1.9	[c]	2.09	[c]	
		(Pd)P	[c]	548	[c]	1670	151
DPB	4H	free base	11.7	–	17.0[18]	–	–
	Pd, 2H	free base	11.5	–	13.2	–	
		(Pd)P	[c]	368	[c]	1690	133
	Pt, 2H	free base	[c]	–	–	224	
		(Pt)P	–	24	–	122	840
	2Pd	(Pd)P	[c]	258	[c]	2170	–
	2Pt	(Pt)P	–	32	–	136	–

[a] Measured in 2-MeTHF. [b] The uncertainties in the values of the lifetimes are ±10%. [c] The signal is too weak to measure.

H_2DPX, and H_2DPB.[18] In addition, the absorption and fluorescence spectral signatures indicated a significant increase in bandwidth as the C_{meso}–C_{meso} distances decreased. So, for

the series described in this work, the lowest-energy triplet state undergoes two molecular dynamics processes: 1) distortions (a torsional distortion along the C_{meso}–C_{aryl} bond and nonplanar distortion of the porphyrin framework) and 2) inter-macrocycle interactions. Their effects on τ_P are opposite. To reduce the effect of the former dynamic process, the photophysical properties were also examined at 77 K.[52]

Comparison of the τ_P [(Pd)P] data for the mono-metalated (Pd)H_2DPS, (Pd)H_2DPX, and (Pd)H_2DPB systems with those for the dimetalated bisporphyrins indicates the presence of an additional deactivation process. The τ_P data for (Pd)P, (Pd)$_2$DPS, (Pd)$_2$DPX, and (Pd)$_2$DPB are 1870, 1920, 2240, and 2170 μs, showing a much attenuated trend. In the heteronuclear systems [(Pd)H_2 and (PdZn)], the (Pd)P data at 298 K (Figure 9a) shows the same trend as the palladium homonuclear systems discussed above. However, the analysis is blurred by the dominant torsional molecular dynamic processes described above ($k_{nr} \gg k_{ET}$, nr = nonradiative). Figure 9b and the data in Table 5 allow the τ_P data measured for the (Pd)$_2$ and (Pd)H_2 series at 77 K to be compared. The values of τ_P for (Pd)$_2$DPS, (PdZn)DPS, and (Pd)H_2DPS are almost identical, indicating that no energy transfer occurs in (PdZn)DPS and (Pd)H_2DPS. However, the fact that τ_P[(Pd)H_2DPX] < τ_P[(Pd)$_2$DPX] and τ_P[(PdZn)DPX] < τ_P[(Pd)$_2$DPX] indicate that T_1–T_1 energy transfer occurs [^{3}(Pd)P → ^{3}(Zn)P and ^{3}(Pd)P → ^{3}H$_2$P].[53]

Evidence for T–T energy transfer: To further demonstrate the presence of T_1–T_1 transfer, the platinum analogues were investigated.[45] Based on the absorption (Figure 3c) and emission data (Figure 7), the donor and acceptor are
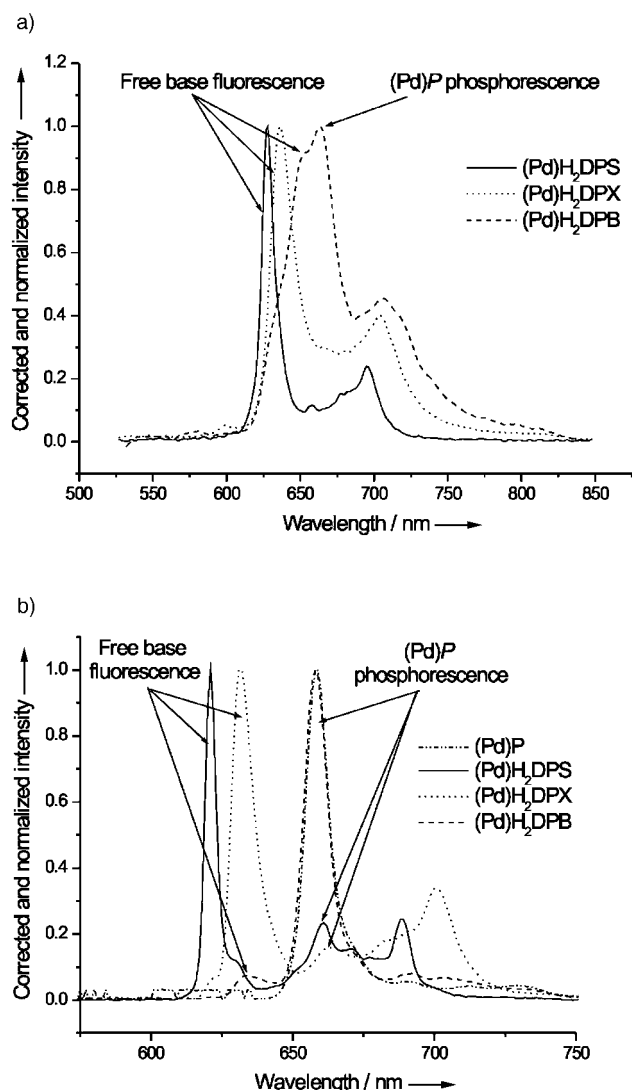
a)

b)

Figure 4. Emission spectra of (Pd)H$_2$-bisporphyrins in 2-MeTHF at a) 298 and b) 77 K ($\lambda_{\text{excitation}}$ = 510 nm).
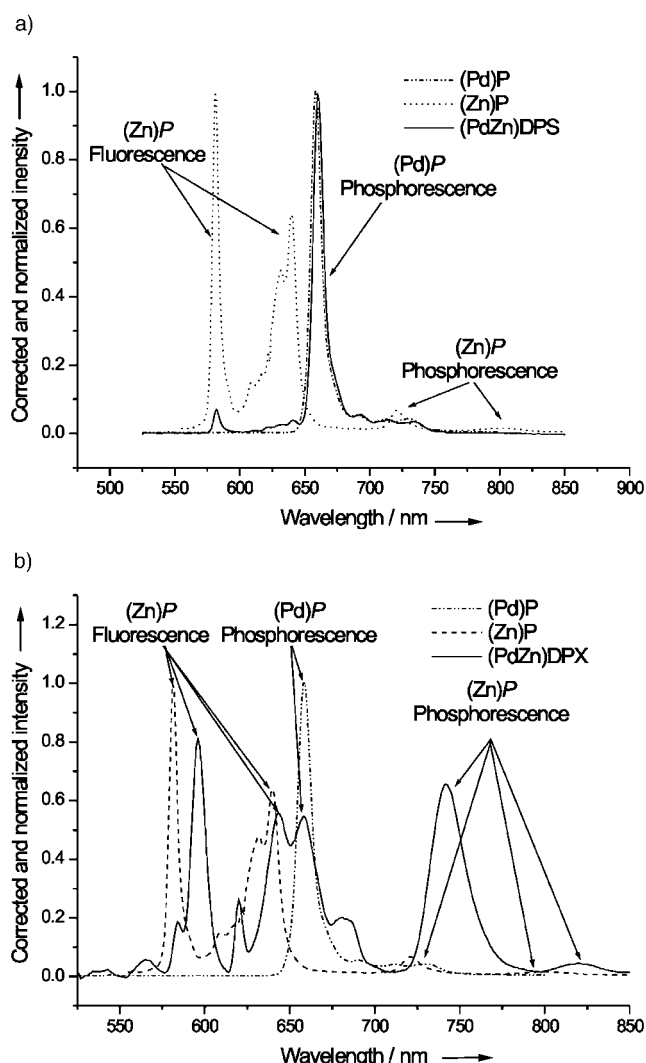
a)

b)

Figure 6. Emission spectra of a) (PdZn)DPS and b) (PdZn)DPX in comparison with the spectra of the two monoporphyrins (Zn)P and (Pd)P (2-MeTHF, 77 K, $\lambda_{\text{excitation}}$ = 510 nm).
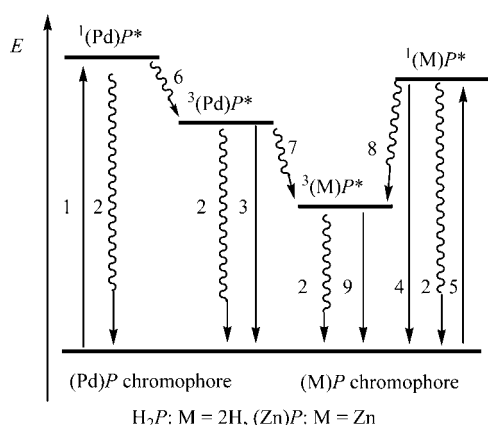

Figure 5. Energy diagram for the (PdM) bisporphyrins (M = H$_2$, Zn). 1, 5: absorption S$_0$–S$_1$; 2: nonradiative deactivation (NR); 3: (Pd)P phosphorescence; 4: M = 2H, Zn; (M)P fluorescence; 6, 8: intersystem crossing (ISC); 9: M = Zn; (Zn)P phosphorescence; 7: triplet–triplet energy transfer.

the (Pt)P and H$_2$P chromophores, respectively. In this case, the acceptor turns out to be phosphorescent. The emission spectra of (Pt)H$_2$DPX and (Pt)H$_2$DPB exhibit a strong phosphorescence at 650 nm due to (Pt)P and a weaker phosphorrescence at 800 nm and above due to H$_2$P. The excitation spectra of the 650 nm phosphorescence is characteristic of the (Pt)P chromophore as these spectra superpose the absorption of PtP, (Pt$_2$)DPX, and (Pt$_2$)DPS (Figure 10). On the other hand the excitation spectra of the 800 nm phosphorescence exhibits the anticipated signal for the H$_2$P chromophore at about 570 nm, but also strong signals at 500–510 and 530–540 nm that are associated with the (Pt)P chromophore. At 800 nm, there is practically no more (Pt)P phosphorescence. The strong peaks associated with the (Pt)P chromophore in the excitation spectra of the H$_2$P phosphorrescence can only be due to triplet–triplet energy transfer.
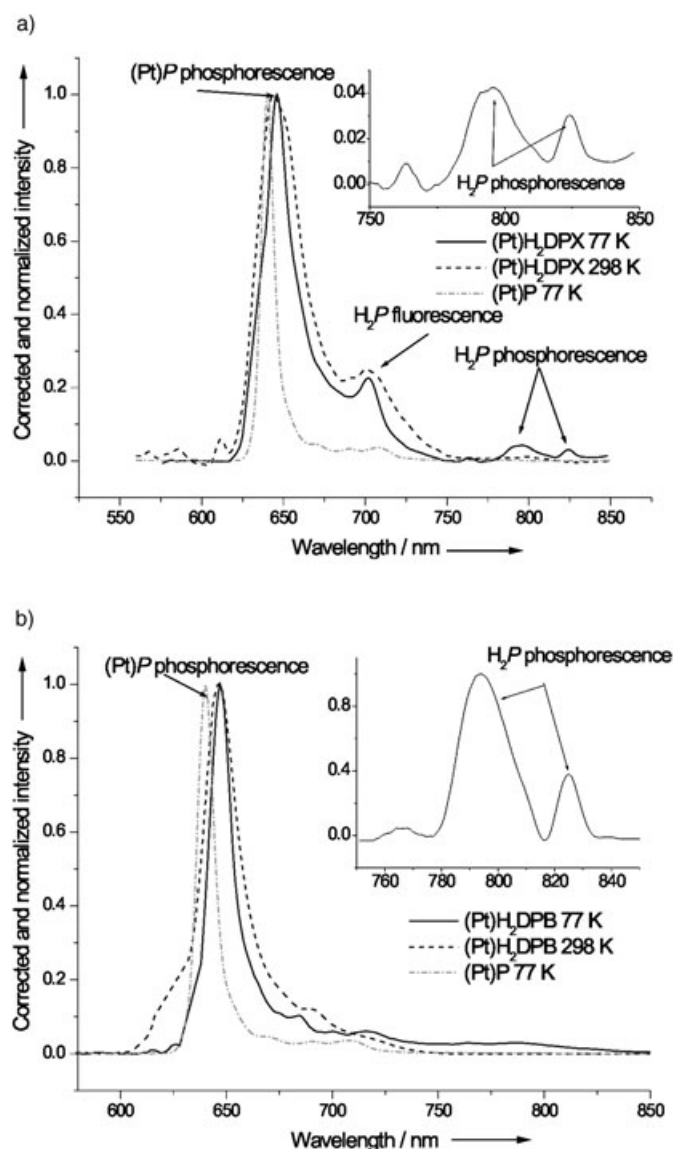
a)

b)

Figure 7. Emission spectra at 298 and 77 K of a) (Pt)H₂DPX and b) (Pt)H₂DPB in comparison with the spectra of (Pt)P at 77 K (2-MeTHF, $\lambda_{\text{excitation}} = 510$ nm).

Interaction between the two macrocycles
heavy atom effect

Figure 8. Lifetime of H₂P chromophore in (M)H₂DPS, (M)H₂DPX, and (M)H₂DPB, where M = H₂ and Pd (298 and 77 K, 2-MeTHF).

a)

b)

Figure 9. Lifetime of the (Pd)P chromophore of P, DPS, DPX, and DPB systems at a) 298 K and b) 77 K in 2-MeTHF.

Energy transfer determination: The rate constants for triplet–triplet energy transfer, k_{ET}, were calculated from Equation (1), where τ_P and τ_P^0 are the phosphorescence lifetimes of the (Pd)P or (Pt)P chromophore of the hetero- [(Pd)H₂, (Pt)H₂, and (PdZn)] and homometallic bisporphyrins [(Pd)₂ and (Pt)₂] systems, respectively (Table 5).

$$k_{\text{ET}} = \left(\frac{1}{\tau_P} - \frac{1}{\tau_P^0} \right) \tag{1}$$

Mechanisms: There are two possible general mechanisms for energy transfer: 1) the Förster (dipole–dipole interaction) and 2) the Dexter (electronic exchange) mechanisms.[20,35] Our previous investigation indicated that S₁–S₁
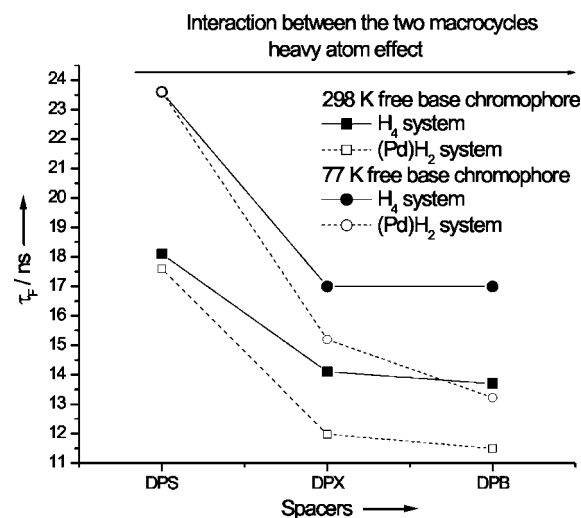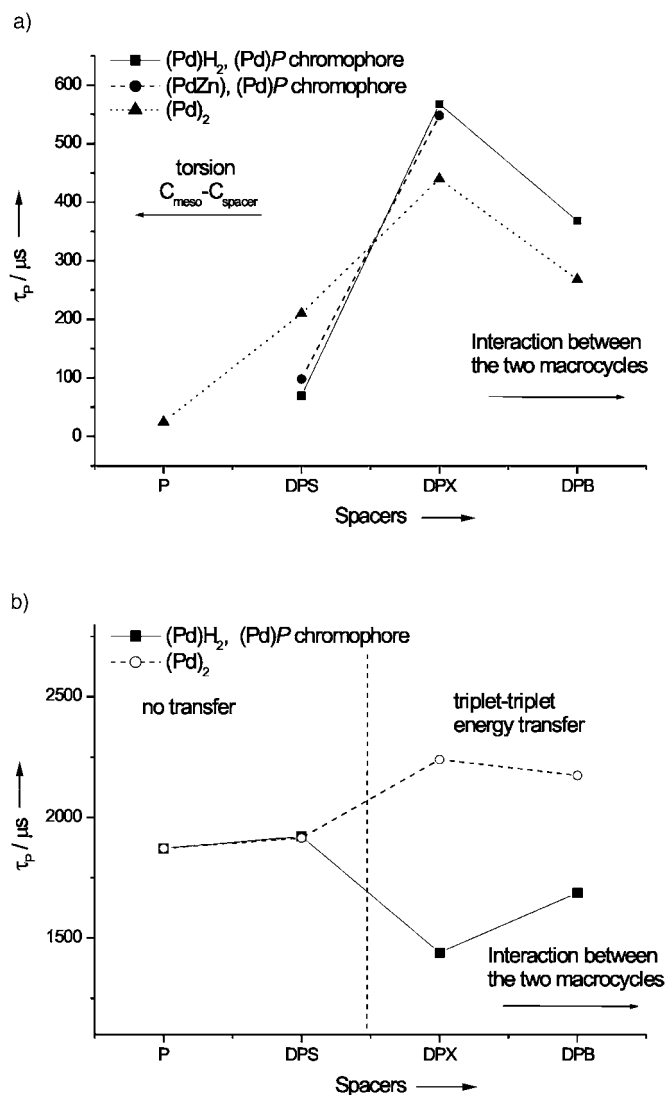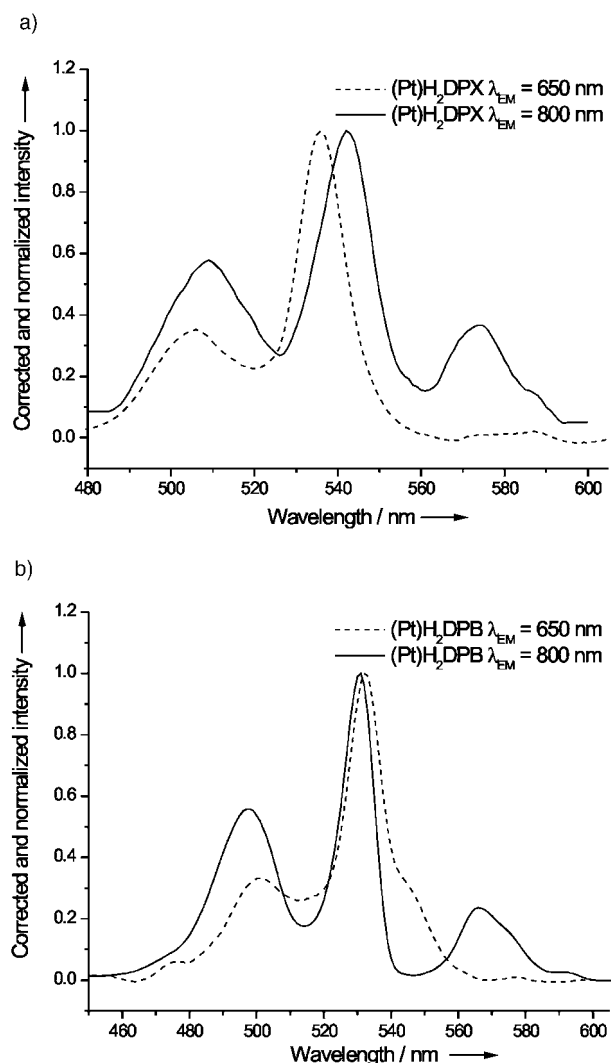
a)

b)

Figure 10. Excitation spectra at 77 K of a) (Pt)H$_2$DPX and b) (Pt)H$_2$DPB ($\lambda_{emission}$ = 650 and 800 nm, 2-MeTHF).

and porphyrin rings are perpendicular, as depicted in the X-ray structure for example, disfavors the electron exchange process. Second, because the electron density at the *meso*-carbon atom is zero or minimal for β-substituted macrocycles based on reported theoretical calculations, the probability for efficient electronic and orbital "communication" between the spacer and rings is also very unlikely. A convincing mechanistic argument comes from the experimentally measured rate constants for the DPX and DPS systems. While energy transfer occurs at a measurable rate in the former donor–acceptor molecule, it does not in the latter, even though the number of chemical bonds between the two connected *meso*-carbons is the same. It is difficult to compare the reported data as the macrocycles have different substitution patterns. In addition, the metals differ and their effect on energy transfer, whether singlet or triplet, is also unknown.

Conclusions

In order to explain the unusual photophysical properties of the (Pd)*P* chromophore in the face-to-face homo- and heteronuclear bisporphyrins, an excited distorted structure in the triplet state must be invoked.[34,50,51] The data for the heteronuclear bisporphyrins at 298 and 77 K are very different as excited-state distortional molecular dynamics are very important at room temperature, precluding intramolecular T$_1$–T$_1$ energy transfer between the (Pd)*P* donor and H$_2$*P* or (Zn)*P* acceptor ($k_{ET} \ll k_{nr}$ at 298 K) as small k_{ET} values were measured for (Pd)H$_2$DPX, (PdZn)DPX, and (Pd)H$_2$DPB. The results indicate that the critical C$_{meso}$–C$_{meso}$ distance at which the Dexter mechanism is no longer efficient is somewhere between the C$_{meso}$–C$_{meso}$ distance in the DPS and DPX systems and agree with a previous report on S$_1$–S$_1$ energy transfer for the same spacers.[12] These bismacrocyclic systems can be viewed as rigid models for "molecular switches" for T$_1$–T$_1$ energy transfer (and heavy-atom effects) which is controlled by the C$_{meso}$–C$_{meso}$ distance.

We are currently developing flexible spacers such as calix[4]arenes[69–76] that would respond to stimuli either bringing the donor and the acceptor closer together leading to a quenching of the donor emission, or separating them rendering the molecular device luminescent. In this way, an "on–off" molecular device can be designed to take advantage of the energy-transfer processes either in the singlet states for lighter-element systems or in the triplet states for heavier-atom-containing molecules.

energy transfer in (Zn)H$_2$DPS occurs predominantly by the Förster mechanism, while in (Zn)H$_2$DPX and (Zn)H$_2$DPB, the Dexter process is mainly effective[12] as a result of the C$_{meso}$–C$_{meso}$ distance. In this work, there is evidence for T$_1$–T$_1$ transfer in (Pd)H$_2$DPX and (Pd)H$_2$DPB [and (PdZn)DPX], but not in the DPS series. These findings are consistent with T$_1$–T$_1$ energy transfer occurring only by the Dexter mechanism. The critical C$_{meso}$–C$_{meso}$ distance at which the Dexter process is no longer efficient is somewhere between 4.3 (DPX) and 6.3 Å (DPS). This is perfectly consistent with the results obtained for S$_1$–S$_1$ energy transfer, which showed this distance to be around 5–6 Å.

Comparison with the literature: The k_{ET} data for T$_1$–T$_1$ energy transfer in these molecules are amongst the lowest known (see the Supporting Information).[6,23,25,54–60] Two mechanisms may be addressed; through-bond and through-space energy transfer. Two arguments rule out the former process. First, the fact that the π systems of the rigid spacer

Experimental Section

purchased from Janssen Chimica and $PtCl_2$ from Johnson Mathey. Column chromatography was performed with neutral alumina (Merck; usually Brockmann Grade III, deactivated with 6% water) and silica gel (Merck; 70–120 mm) and monitored by thin-layer chromatography (Merck 60 F254 silica gel precoated sheets, 0.2 mm thick) and UV/Vis spectroscopy.

Apparatus: ^{1}H NMR spectra were recorded with a Bruker DRX-500 AVANCE spectrometer at the Centre de Spectrométrie Moléculaire de l'Université de Bourgogne. Microanalyses were performed at the Université de Bourgogne using a Fisons EA 1108 CHNS instrument. UV/Vis spectra were recorded with a Varian Cary 50 spectrophotometer. Mass spectra were obtained in linear mode with a Bruker Proflex III MALDI-TOF mass spectrometer using dithranol as the matrix. Emission and excitation spectra were obtained by using a double monochromator Fluorolog 2 instrument from Spex. Fluorescence lifetimes were measured on a Timemaster Model TM-3 apparatus from PTI. The source was a nitrogen laser equipped with a high-resolution dye laser (FWHM ~ 1500 ps) and the fluorescence lifetimes were obtained by deconvolution and distribution lifetime analysis.[20] All of the samples were prepared under an inert atmosphere (in a glove box, $P_{O_2} < 1$–3 ppm; all of the molecules studied were oxygen sensitive at 298 K[20,32]) by dissolution of the different compounds in 2-MeTHF in 1-cm^3 quartz cells equipped with a septum (298 K) or in standard 5-mm NMR tubes (77 K). Three different measurements (i.e., different solutions) were performed for each photophysical data (quantum yields and lifetimes). The sample concentrations were chosen to obtain an absorbance of about 0.05. Each absorbance value was measured five times to gain better accuracy in the measurement of the quantum yields. The quantum yield of H_2TPP ($\Phi = 0.11$) was used as a reference for the quantum yields measured at 298 K.[27,42,63] The quantum yield of H_2TPP ($\Phi = 0.11$) was also used as reference for the quantum yields measured at 77 K, which itself was obtained by using (Pd)TPP ($\Phi = 0.17$; 77 K; MCH = methylcyclohexane) as reference.[43,64]

Crystallography: Red, single crystals of (Pd)H_2DPX, which exhibit a plate morphology, were grown from CH_2Cl_2/heptane diffusion. A high-quality specimen of approximately $0.10 \times 0.37 \times 0.50$ mm^3 was selected for the X-ray diffraction experiment. Data were collected[65] on an Enraf–Nonius KappaCCD diffractometer equipped with a low-temperature nitrogen jet stream system (Oxford Cryosystems) at $T = 110(2)$ K. Unit cell parameters were obtained from a least-squares refinement by using the setting angles of all the collected reflections ($\theta_{max} = 27.4°$). The intensity data were recorded as ϕ and ω scans with κ offsets. Data reduction was performed by using the DENZO program.[66] The space group was determined on the basis of systematic absences, packing considerations, a statistical analysis of the intensity distribution, and the successful solution and refinement of the structure.

The structure was solved by using direct methods[67] and refined by full-matrix least-squares on F^2 with a complete set of reflections.[68] Anisotropic thermal parameters were used to refine the non-hydrogen atoms. Hydrogen atoms were located by Fourier synthesis and placed at calculated positions by using a riding model, except those bonded to nitrogen atoms which were not found. All the hydrogen atoms were refined by using a global isotropic temperature factor. The metal atom was found to be disordered over two positions, lying in the mean 4 N plane of each porphyrin moiety in the centre of the macrocycle cavity. The site occupation factors (SOFs) corresponding to these positions are 0.532(1) and 0.468(1). Two $C_{pyrrole}$ and one C_{meso} atoms, as well as two ethyl groups (all belonging to the porphyrin moiety for which palladium has a SOF of 0.532(1)) were also found to be disordered and occupying two positions. For the $C_{pyrrole}$ and C_{meso} atoms, the SOFs are 0.58(2) and 0.42(2). For both the ethyl groups, the SOFs are 0.51(1) and 0.49(1). Table 1 shows the crystal data and some experimental and refinement details.

CCDC-249573 contains the supplementary crystallographic data for this paper. These data can be obtained free of charge from The Cambridge Crystallographic Data Centre via www.ccdc.cam.ac.uk/data_request/cif.

General procedure for the preparation of monopalladium bisporphyrins: The monozinc bisporphyrin (1 equiv) was added to a benzonitrile (20 mL) solution of $PdCl_2$ (1.5 equiv). The mixture was stirred under reflux for 1.5 h. The solution was taken to dryness. CH_2Cl_2 was then

added and the solution was vigorously stirred for 5 min and filtered through a pad of silica (CH_2Cl_2/heptane 1:1). The first purple band was collected as the bis-palladium compound and elution was performed with CH_2Cl_2/MeOH (increase of MeOH) in order to collect the monopalladium bisporphyrin. The solvent was removed under vacuum. Recrystallization in CH_2Cl_2/heptane afforded the pure monopalladium derivative as a purple solid.

(Pd)H_2DPS: Yield: 37% (40 mg). ^{1}H NMR (500 MHz, CDCl$_3$): $\delta = 9.83$ (m, 2H), 9.76 (m, 2H), 9.69 (m, 2H), 9.64 (m, 2H), 8.83 (m, 2H), 7.96 (m, 2H), 3.81 (m, 16H), 3.39 (s, 6H), 3.33 (s, 6H), 3.32 (s, 6H), 3.30 (s, 6H), 1.65 (m, 24H), −3.70 ppm (2 s, 2H); elemental analysis calcd (%) for $C_{76}H_{78}N_8PdS \cdot 0.6C_7H_{16}$: C 73.98, H 6.78, N 8.61, S 2.46; found: C 74.33, H 6.42, N 8.92, S 2.44; MS (MALDI-TOF): m/z: 1241; MS (LSIMS): m/z: 1243; calcd for $C_{76}H_{78}N_8PdS$: 1242.

(Pd)H_2DPX: Yield: 43% (43 mg). ^{1}H NMR (500 MHz, CDCl$_3$): $\delta = 9.24$ (m, 1H), 9.14 (s, 1H), 8.44 (m, 2H), 8.32 (m, 2H), 7.93 (m, 2H), 7.25 (m, 2H), 7.07 (m, 2H), 4.16 (m, 4H), 3.79 (m, 4H), 3.39 (m, 4H), 3.30 (m, 4H), 3.18 (s, 6H), 3.09 (s, 6H), 2.30 (m, 18H), 1.74 (m, 12H), 1.40 (m, 12H), −6.62 ppm (2 s, 2H); elemental analysis calcd (%) for $C_{79}H_{84}N_8OPd \cdot MeOH$: C 73.91, H 6.82, N 8.62; found: C 73.87, H 6.76, N 8.45; MS (MALDI-TOF): m/z: 1266; calcd for $C_{79}H_{84}N_8OPd$: 1266.

(Pd)H_2DPB: Yield: 53% (120 mg). ^{1}H NMR (500 MHz, CDCl$_3$): $\delta = 9.11$ (s, 1H), 8.77 (s, 1H), 8.44 (m, 4H), 7.20 (d, 2H, $J = 7.4$ Hz), 6.95 (t, $J = 7.4$ Hz, 2H), 6.77 (d, $J = 6.4$ Hz, 2H), 4.16 (qd, 2H), 4.03 (qd, 2H), 3.88 (qd, 2H), 3.72 (m, 6H), 3.52 (m, 4H), 3.26 (s, 6H), 3.13 (s, 6H), 2.95 (s, 6H), 2.85 (s, 6H), 1.77 (t, 6H), 1.61 (t, 6H), 1.40 (t, 6H), 1.35 (t, 6H), −7.27 (s, 1H), −7.70 ppm (s, 1H); elemental analysis calcd (%) for $C_{76}H_{78}N_8Pd$: C 75.44, H 6.50, N 9.26; found: C 75.63, H 6.77, N 9.00; MS (MALDI-TOF): m/z: 1209; calcd for $C_{76}H_{78}N_8Pd$: 1209.

General procedure for the preparation of monoplatinum bisporphyrins: The monozinc bisporphyrin (1 equiv) was dissolved in benzonitrile (50 mL). $PtCl_2$ (1.1 equiv) was added and the solution was refluxed under argon for two hours. The solvent was evaporated to dryness and the residue purified by alumina chromatography (CH_2Cl_2/heptane, 3:7). The second band was collected and the solvent evaporated. Recrystallization in CH_2Cl_2/heptane afforded the monoplatinum derivative as a red solid.

(Pt)H_2DPX: Yield: 66% (250 mg). ^{1}H NMR (500 MHz, CDCl$_3$): $\delta = 9.52$ (m, 1H), 8.90 (m, 1H), 8.38 (s, 2H), 8.12 (d, $J = 7.5$ Hz, 2H), 7.99 (d, $J = 8.6$ Hz, 2H), 7.40 (m, 2H), 7.16 (m, 2H), 4.25 (m, 4H), 3.76 (m, 4H), 3.40 (m, 4H), 3.33 (m, 4H), 3.15 (s, 6H), 2.42 (m, 6H), 2.26 (m, 12H), 1.73 (m, 6H), 1.51 (m, 12H), 1.38 (m, 6H), −6.51 ppm (br, 2H); elemental analysis calcd (%) for $C_{79}H_{84}N_8OPt \cdot 6CH_2Cl_2$: C 54.70, H 5.18, N 6.00; found: C 54.52, H 4.79, N 6.62; MS (MALDI-TOF): m/z: 1356; calcd for $C_{79}H_{84}N_8OPt$: 1357.

(Pt)H_2DPB: Yield: 61% (94 mg). ^{1}H NMR (500 MHz, CDCl$_3$): $\delta = 9.14$ (s, 1H), 8.68 (s, 1H), 8.51 (s, 2H), 8.37 (s, 2H), 7.20 (m, 2H), 6.98 (m, 3H), 6.77 (d, $J = 8.1$ Hz, 1H), 4.37 (m, 4H), 3.90 (m, 4H), 3.78 (m, 4H), 3.56 (m, 4H), 3.31 (s, 6H), 3.11 (s, 6H), 2.93 (s, 6H), 2.87 (s, 6H), 1.77 (t, $J = 7.7$ Hz), 1.60 (t, $J = 7.9$ Hz, 6H), 1.39 (m, 12H), −7.28 (s, 1H), −7.78 ppm (s, 1H); elemental analysis calcd (%) for $C_{76}H_{78}N_8Pt \cdot 2CH_2Cl_2$: C 63.79, H 5.62, N 7.63; found: C 62.79, H 5.56, N, 7.56; MS (MALDI-TOF): m/z: 1299; calcd for $C_{76}H_{78}N_8Pt$: 1299.

General procedure for the preparation of palladium–zinc bisporphyrins: A saturated solution of $Zn(OAc)_2 \cdot 2H_2O$ in methanol (2 mL) was added to a dichloromethane (10 mL) and triethylamine (1 mL) solution of monopalladium bisporphyrin (0.04 mmol). The mixture was stirred under reflux and the reaction was monitored by UV/Vis spectroscopy and TLC. Heating was stopped when the starting monopalladium porphyrin was no longer present in the reaction mixture according to TLC (~ 10 min). The solvent was removed under vacuum. The solid was dissolved in CH_2Cl_2 and purified by chromatography (silica, CH_2Cl_2/heptane, 1:1). Recrystallization in CH_2Cl_2/heptane afforded the pure palladium–zinc derivative as a purple solid.

(PdZn)DPS: Yield: 76% (40 mg). ^{1}H NMR (500 MHz, CDCl$_3$): $\delta = 9.88$ (s, 2H), 9.79 (s, 2H), 9.75 (m, 2H), 9.71 (m, 2H), 8.85 (m, 2H), 7.97 (m, 2H), 3.78 (m, 16H), 3.42 (s, 6H), 3.37 (s, 6H), 3.35 (m, 6H), 3.31 (s, 6H), 1.64 ppm (m, 24H); elemental analysis calcd (%) for $C_{76}H_{76}N_8PdSZn$: C

69.93, H 5.87, N 8.58, S 2.46; found: C 69.90, H 5.78, N 8.95, S 2.46; MS (MALDI-TOF): m/z: 1302; calcd for $C_{76}H_{76}N_8PdSZn$: 1302.

(PdZn)DPX: Yield: 76% (41 mg). ^{1}H NMR (500 MHz, CDCl$_3$): $\delta = 9.06$ (m, 2H), 8.60 (m, 2H), 8.42 (m, 2H), 7.83 (m, 2H), 7.18 (m, 2H), 6.85 (m, 2H), 4.17 (m, 4H), 3.89 (m, 4H), 3.57 (m, 4H), 3.43 (m, 4H), 3.25 (m, 12H), 2.27 (m, 18H), 1.71 (m, 12H), 1.45 ppm (m, 12H); elemental analysis calcd (%) for $C_{79}H_{82}N_8OPdZn\cdot0.6C_7H_{16}$: C 71.64, H 6.50, N 8.17; found: C 71.67, H 6.48, N 8.42; MS (MALDI-TOF): m/z: 1329; MS (LSIMS): m/z: 1333; calcd for $C_{79}H_{82}N_8OPdZn$: 1328.

Procedure for the preparation of (Pd)$_2$DPB: H$_4$DPB (300 mg, 0.27 mmol) was added to a benzonitrile (40 mL) solution of PdCl$_2$ (200 mg, 1 mmol). After stirring the mixture under reflux for 1 h, the solvent was removed under vacuum. CH$_2$Cl$_2$ (20 mL) was then added and the solution was vigorously stirred for 5 min and filtered through a pad of silica (CH$_2$Cl$_2$/heptane, 5:8). The bispalladium compound was collected as the first purple band. The solvent was removed under vacuum. Recrystallization in CH$_2$Cl$_2$/MeOH afforded (Pd)$_2$DPB as a purple solid.

(Pd)$_2$DPB: Yield: 66% (235 mg). ^{1}H NMR (500 MHz, CDCl$_3$): $\delta = 8.93$ (s, 2H), 8.53 (s, 4H), 7.18 (d, 2H), 6.99 (t, 2H), 6.88 (d, 2H), 4.16 (m, 4H), 3.84 (m, 8H), 3.57 (m, 4H), 3.35 (m, 12H), 2.99 (m, 12H), 1.67 (m, 12H), 1.41 ppm (m, 12H); elemental analysis calcd (%) for $C_{76}H_{76}N_8Pd_2\cdot MeOH$: C 68.69, H 5.99, N 8.32; found: C 68.99, H 6.53, N 8.23; MS (MALDI-TOF): m/z: 1312; calcd for $C_{76}H_{76}N_8Pd_2$: 1312.

General procedure for the preparation of bisplatinum bisporphyrins and monoplatinum porphyrin: The monozinc bisporphyrin (1 equiv) was dissolved in benzonitrile (50 mL). PtCl$_2$ (4.3 equiv) was added and the solution refluxed under argon for 2 h. The solvent was evaporated under vacuum and the residue was purified by alumina chromatography (CH$_2$Cl$_2$/heptane, 3:7). The second band was collected and the solvent evaporated. Recrystallization in CH$_2$Cl$_2$/heptane afforded the bisplatinum derivative as a red solid.

(Pt)$_2$DPX: Yield: 67% (179 mg). ^{1}H NMR (500 MHz, CDCl$_3$): $\delta = 9.01$ (s, 2H), 8.42 (s, 4H), 7.85 (d, $J = 8.8$ Hz, 2H), 7.23 (t, $J = 7.9$ Hz, 2H), 7.02 (d, $J = 7.9$ Hz, 2H), 4.11 (m, 4H), 3.81 (m, 4H), 3.56 (m, 4H), 3.32 (m, 4H), 3.23 (s, 12H), 2.26 (s, 12H), 2.19 (s, 6H), 1.70 (t, $J = 7.7$ Hz, 12H), 1.40 ppm (t, $J = 7.6$ Hz, 12H); elemental analysis calcd (%) for $C_{79}H_{82}N_8OPt_2$: C 61.23, H 5.33, N 7.23; found: C 61.37, H 5.40, N 7.16; MS (MALDI-TOF): m/z: 1549; calcd for $C_{79}H_{82}N_8OPt_2$: 1550.

(Pt)$_2$DPB: Yield: 72% (31 mg). ^{1}H NMR (500 MHz, [D$_6$]DMSO, 340 K): $\delta = 8.91$ (s, 2H), 8.54 (s, 4H), 7.31 (d, $J = 6.8$ Hz, 2H), 7.08 (t, $J = 7.3$ Hz, 2H), 6.86 (d, $J = 7.7$ Hz, 2H), 4.07 (m, 4H), 3.82 (m, 4H), 3.55 (m, 4H), 3.26 (s, 12H), 3.15 (m, 12H), 1.65 (t, $J = 7.8$ Hz, 12H), 1.39 ppm (t, $J = 7.6$ Hz, 12H); elemental analysis calcd (%) for $C_{76}H_{76}N_8Pt_2$: C 61.20, H 5.14, N 7.51; found: C 61.01, H 5.30, N 7.29; MS (MALDI-TOF): m/z: 1493; calcd for $C_{76}H_{76}N_8Pt_2$: 1492.

(Pt)P: Yield: 75% (68 mg). ^{1}H NMR (500 MHz, CDCl$_3$): $\delta = 10.00$ (s, 2H), 9.97 (s, 1H), 8.03 (d, $J = 6.8$ Hz, 2H), 7.77 (t, $J = 7.7$ Hz, 1H), 7.71 (t, $J = 7.0$ Hz, 2H), 4.00 (q, $J = 7.6$ Hz, 4H), 3.90 (q, $J = 7.8$ Hz, 4H), 3.56 (s, 6H), 2.38 (s, 6H), 1.87 (t, $J = 8.0$ Hz, 6H), 1.73 ppm (t, $J = 7.7$ Hz, 6H); elemental analysis calcd (%) for $C_{38}H_{40}N_4Pt\cdot2CH_2Cl_2\cdot2C_7H_{15}$: C 58.11, H 6.68, N 5.02; found: C 58.33, H 6.90, N 5.38; MS (MALDI-TOF): m/z: 747; calcd for $C_{38}H_{40}N_4Pt$: 748.

Acknowledgements

[1] P. Jordan, P. Fromme, H. T. Witt, O. Klukas, W. Saenger, N. Krauss, *Nature* **2001**, *411*, 909–917.

[2] D. Gust, T. A. Moore, A. L. Moore, *Acc. Chem. Res.* **2001**, *34*, 40–48.

[3] G. Kodis, P. A. Liddell, L. de la Garza, P. C. Clausen, J. S. Lindsey, A. L. Moore, T. A. Moore, D. Gust, *J. Phys. Chem. A* **2002**, *106*, 2036–2048.

[4] C. Luo, D. M. Guldi, H. Imahori, K. Tamaki, Y. Sakata, *J. Am. Chem. Soc.* **2000**, *122*, 6535–6551.

[5] D. Gust, T. A. Moore, A. L. Moore, *Acc. Chem. Res.* **1993**, *26*, 198–205.

[6] P. D. Harvey in *The Porphyrin Handbook*, Vol. 18 (Eds.: K. M. Kadish, K. M. Smith, R. Guilard), Academic Press, San Diego, **2003**, pp. 63–250.

[7] N. Aratani, A. Osuka, H. S. Cho, D. Kim, *J. Photochem. Photobiol. C* **2002**, *3*, 25–52.

[8] R. A. Agbaria, P. B. Oldham, M. McCarroll, L. B. McGown, I. M. Warner, *Anal. Chem.* **2002**, *74*, 3952–3962.

[9] D. Holten, D. F. Bocian, J. S. Lindsey, *Acc. Chem. Res.* **2002**, *35*, 57–69.

[10] O. S. Wolfbeis, *Anal. Chem.* **2002**, *74*, 2663–2678.

[11] R. K. Lammi, R. W. Wagner, A. Ambroise, J. R. Diers, D. F. Bocian, D. Holten, J. S. Lindsey, *J. Phys. Chem. B* **2001**, *105*, 5341–5352.

[12] S. Faure, C. Stern, R. Guilard, P. D. Harvey, *J. Am. Chem. Soc.* **2004**, *126*, 1253–1261.

[13] T. Förster, *Ann. Phys.* **1948**, *2*, 55–73.

[14] T. Förster, *Naturwissenschaften* **1946**, *33*, 166–175.

[15] D. L. Dexter, *J. Chem. Phys.* **1953**, *21*, 836–850.

[16] The crystal structure of (Zn)$_2$DPS has also been investigated but the presence of significant disorder in the solvent molecules between the macrocycles makes this structure unsatisfactory for a full report. However, preliminary data allow the following information to be extracted: monoclinic ($P2_1/m$), $a = 13.059(3)$, $b = 28.0973(6)$, $c = 21.3934(5)$ Å, $\beta = 96.981(1)°$, $V = 7791.7(3)$ Å^3, $Z = 4$, $R_1 = 0.991$, $wR_2 = 0.2064$ ($I > 2\sigma(I)$), and $R_1 = 0.1739$, $wR_2 = 0.2365$ (all data). Two crystallographically independent molecules are found in the lattice (Mol A and Mol B). The values of $d(C_{meso}-C_{meso})$ are 6.249 and 6.412 Å (average = 6.33 Å), and the values of $d(Ct–Ct)$ are 9.177 and 9.622 Å (average = 9.40 Å), respectively. The V-shaped bismacrocycles Mol A and Mol B stack side-by-side alternating right-way-up and upside-down, forming an infinite 1D structure in which p contacts occur. The Mol A–Mol B distance [$d(Ct–Ct)$] is 5.594 Å.

[17] C. J. Chang, E. A. Baker, B. J. Pistorio, Y. Deng, Z.-H. Loh, S. E. Miller, S. D. Carpenter, D. G. Nocera, *Inorg. Chem.* **2002**, *41*, 3102–3109.

[18] F. Bolze, C. P. Gros, M. Drouin, E. Espinosa, P. D. Harvey, R. Guilard, *J. Organomet. Chem.* **2002**, *643–644*, 89–97.

[19] F. Bolze, M. Drouin, P. D. Harvey, C. P. Gros, E. Espinosa, R. Guilard, *J. Porphyrins Phthalocyanines* **2003**, *7*, 474–483.

[20] B. Valeur, *Molecular Fluorescence. Principles and Applications*, Wiley-VCH, Weinheim, **2002**.

[21] A. Prodi, M. T. Indelli, C. J. Kleverlaan, F. Scandola, E. Alessio, T. Gianferrara, L. G. Marzilli, *Chem. Eur. J.* **1999**, *5*, 2668–2679.

[22] L. Flamigni, F. Barigelletti, N. Armaroli, B. Ventura, J.-P. Collin, J.-P. Sauvage, J. A. G. Williams, *Inorg. Chem.* **1999**, *38*, 661–667.

[23] M. Asano-Someda, Y. Kaizu, *Inorg. Chem.* **1999**, *38*, 2303–2311.

[24] O. Ohno, Y. Ogasawara, M. Asano, Y. Kajii, Y. Kaizu, K. Obi, H. Kobayashi, *J. Phys. Chem.* **1987**, *91*, 4269–4273.

[25] A. Kyrychenko, B. Albinsson, *Chem. Phys. Lett.* **2002**, *366*, 291–299.

[26] A. Harriman, F. M. Romero, R. Ziessel, A. C. Benniston, *J. Phys. Chem. A* **1999**, *103*, 5399–5408.

[27] M. Gouterman in *The Porphyrins*, Vol. III (Ed.: D. Dolphin), Academic Press, New York, **1978**, pp. 1–165.

[28] P. J. Spellane, M. Gouterman, A. Antipas, S. Kim, Y. C. Liu, *Inorg. Chem.* **1980**, *19*, 386–391.

[29] J. A. Shelnutt, V. Ortiz, *J. Phys. Chem.* **1985**, *89*, 4733–4739.

[30] J. T. Fletcher, M. J. Therien, *J. Am. Chem. Soc.* **2002**, *124*, 4298–4311.

[31] I. Okura, *J. Porphyrins Phthalocyanines* **2002**, *6*, 268–270.

[32] F. Bolze, C. P. Gros, P. D. Harvey, R. Guilard, *J. Porphyrins Phthalocyanines* **2001**, *5*, 569–574.

[33] M. Sinaasappel, C. Ince, *J. Appl. Physiol.* **1996**, *81*, 2297–2303.

[34] Z.-H. Loh, S. E. Miller, C. J. Chang, S. D. Carpenter, D. G. Nocera, *J. Phys. Chem. A* **2002**, *106*, 11700–11708.

[35] N. J. Turro, *Modern Molecular Photochemistry*, University Science Books, Sausalito, California, **1991**.

[36] R. Guilard, M. A. Lopez, A. Tabard, P. Richard, C. Lecomte, S. Brandès, J. E. Hutchison, J. P. Collman, *J. Am. Chem. Soc.* **1992**, *114*, 9877–9889.

[37] P. D. Harvey, N. Proulx, G. Martin, M. Drouin, D. J. Nurco, K. M. Smith, F. Bolze, C. P. Gros, R. Guilard, *Inorg. Chem.* **2001**, *40*, 4134–4142.

[38] J. P. Fillers, K. G. Ravichandran, I. Abdalmuhdi, A. Tulinsky, C. K. Chang, *J. Am. Chem. Soc.* **1986**, *108*, 417–424.

[39] C. J. Chang, Y. Deng, A. F. Heyduk, C. K. Chang, D. G. Nocera, *Inorg. Chem.* **2000**, *39*, 959–966.

[40] C. J. Chang, Y. Deng, C. Shi, C. K. Chang, F. C. Anson, D. G. Nocera, *Chem. Commun.* **2000**, 1355–1356.

[41] F. Bolze, Ph.D. Thesis, University of Burgundy (Dijon, France), **2001**.

[42] P. G. Seybold, M. Gouterman, *J. Mol. Spectrosc.* **1969**, *31*, 1–13.

[43] A. Harriman, *J. Chem. Soc. Faraday Trans. 2* **1981**, *77*, 1281–1291.

[44] M. Gouterman, G.-E. Khalil, *J. Mol. Spectrosc.* **1974**, *53*, 88–100.

[45] The transient T_1–T_n absorption spectra were measured at room temperature by nanosecond flash photolysis at the University of Ottawa (see ref. [46]). The transient spectra of $H_2(P)$, H_4DPS, H_4PPX, and H_4DPB exhibit transient signatures characteristic of the formation of triplet H_2P (see examples in refs. [24] and [47]). Similarly, the transient spectra of $(Pd)P$, $(Pd)_2DPS$, $(Pd)_2DPX$, and $(Pd)_2DPB$ also exhibit features that greatly resemble those of the corresponding free bases which indicates the formation of the triplet state as well. The same features were also observed in the spectra of the donor–acceptor. The similarity between the spectra is, however, important as triplet energy transfer cannot be demonstrated with this technique.

[46] M. A. Miranda, E. Font-Sanchis, J. Pérez-Prieto, J. C. Scaiano, *J. Org. Chem.* **2001**, *66*, 2717–2721.

[47] J. Andréasson, A. Kyrychenko, J. Martensson, B. Albinsson, *Photochem. Photobiol. Sci.* **2002**, *1*, 111–119.

[48] The fluorescence quantum yield data for the related $(Pd)_2DPA$ in 2-MeTHF at 298 and 77 K are 0.000108 and 0.000087 ($\pm 10\%$), respectively, and the fluorescence lifetime data are 432 and 470 (± 50) ps, respectively.

[49] However, energy transfer from the $^1(Zn)P^*$ state to the lower-lying $^3(Pd)P$ state is still possible, but reports in the literature for such a transfer between two states of different multiplicity are very rare.

[50] V. Knyukshto, E. Zenkevich, E. Sagun, A. Shulga, S. Bachilo, *Chem. Phys. Lett.* **1998**, *297*, 97–108.

[51] A. Kyrychenko, J. Andréasson, J. Mårtensson, B. Albinsson, *J. Phys. Chem. B* **2002**, *106*, 12613–12622.

[52] To reduce experimental error due to these phenomena (distortions and interactions), only the 77 K data were used in T–T energy transfer studies. In addition, all the palladium complexes were very

[53] The triplet–triplet energy transfer occurs by the Dexter process.

[54] J. Andréasson, J. Kajanus, J. Mårtensson, B. Albinsson, *J. Am. Chem. Soc.* **2000**, *122*, 9844–9845.

[55] N. Toyama, M. Asano-Someda, T. Ichino, Y. Kaizu, *J. Phys. Chem. A* **2000**, *104*, 4857–4865.

[56] M. Asano-Someda, A. Jinmon, N. Toyama, Y. Kaizu, *Inorg. Chim. Acta* **2001**, *324*, 347–351.

[57] M. Asano-Someda, T. Ichino, Y. Kaizu, *J. Phys. Chem. A* **1997**, *101*, 4484–4490.

[58] A. M. Brun, A. Harriman, V. Heitz, J.-P. Sauvage, *J. Am. Chem. Soc.* **1991**, *113*, 8657–8663.

[59] J. L. Sessler, B. Wang, A. Harriman, *J. Am. Chem. Soc.* **1995**, *117*, 704–714.

[60] K. Kilså, J. Kajanus, J. Mårtensson, B. Albinsson, *J. Phys. Chem. B* **1999**, *103*, 7329–7339.

[61] C. K. Chang, I. Abdalmuhdi, *Angew. Chem.* **1984**, *96*, 154–155; *Angew. Chem. Int. Ed. Engl.* **1984**, *23*, 164–165.

[62] J. P. Collman, J. M. Garner, *J. Am. Chem. Soc.* **1990**, *112*, 166–173.

[63] J.-P. Strachan, S. Gentemann, J. Seth, W. A. Kalsbeck, J. S. Lindsey, D. Holten, D. F. Bocian, *J. Am. Chem. Soc.* **1997**, *119*, 11191–11201.

[64] S. L. Murov, I. Carmichael, G. L. Hug, *Handbook of Photochemistry*, 2nd ed., Marcel Dekker, New York, **1993**.

[65] Collect program, Nonius BV, Delft(The Netherlands), **1998**.

[66] Z. Otwinowski, W. Minor, *Methods Enzymol.* **1997**, *276*, 307.

[67] SIR97 program: A. Altomare, M. C. Burla, M. Camalli, G. L. Cascarano, C. Giacovazzo, A. Guagliardi, A. G. G. Moliterni, G. Polidori, R. Spagna, *J. Appl. Crystallogr.* **1999**, *32*, 115–119.

[68] G. M. Sheldrick, SHELXL-97, Program for the Refinement of Crystal Structures, University of Göttingen, Göttingen (Germany), **1997**.

[69] J.-P. Tremblay-Morin, S. Faure, D. Samar, C. Stern, R. Guilard, P. D. Harvey, *Inorg. Chem.* **2005**, in press.

[70] Z. Asfari, J. Vicens, J. Weiss, *Tetrahedron Lett.* **1993**, *34*, 627–628.

[71] R. G. Khoury, L. Jaquinod, K. Aoyagi, M. M. Olmstead, A. J. Fisher, K. M. Smith, *Angew. Chem.* **1997**, *109*, 2604–2607; *Angew. Chem. Int. Ed. Engl.* **1997**, *36*, 2497–2500.

[72] N. Nakamura, A. Ikeda, L. D. Sarson, S. Shinkai, *Supramol. Chem.* **1998**, *9*, 25–29.

[73] L. Zhang, Y. Zhang, H. Tao, X. Sun, Z. Guo, L. Zhu, *Thin Solid Films* **2002**, *413*, 224–230.

[74] M. Dudic, P. Lhotak, I. Stibor, H. Petrickova, K. Lang, *New J. Chem.* **2004**, *28*, 85–90.

[75] M. Dudic, P. Lhotak, I. Stibor, K. Lang, P. Proskova, *Org. Lett.* **2003**, *5*, 149–152.

[76] M. Dudic, P. Lhotak, I. Stibor, H. Dvorakova, K. Lang, *Tetrahedron* **2002**, *58*, 5475–5482.

oxygen-sensitive at 298 K. Therefore the measurements were performed at the limit of O_2 purity (0.1–0.3 ppm in solution) and the lifetimes could vary a little from day to day, making the investigation very difficult at this temperature.